

Improved Deadbeat Predictive Current Control Combined Sliding Mode Strategy for PMSM Drive System

Yajie Jiang, Wei Xu^{ID}, Senior Member, IEEE, Chaoxu Mu^{ID}, Member, IEEE, and Yi Liu, Member, IEEE

Abstract—To promote the drive performance of permanent magnet synchronous machine (PMSM), such as tracking accuracy of both speed and current, one improved deadbeat-based predictive current control (DPCC) scheme based sliding mode is proposed in this paper. First, one novel PMSM model is derived by considering uncertainties of both parameters and external disturbances. Second, in order to improve the dynamic response of PMSM drive system, both sliding mode control (SMC) and DPCC are employed to control the speed and current, respectively. Third, a unified high-order sliding mode observer is designed for the estimation of disturbances and uncertainties in the speed and current loops. Furthermore, the estimated values are compensated with feedback to the designed SMC and DPCC to increase the speed robustness and current tracking accuracy. Comprehensive simulation and experiments demonstrate that the proposed control strategy is strongly robust to acute variations of load and machine parameters, and it is testified to have better speed and current tracking performance.

Index Terms—Deadbeat-based predictive current control (DPCC), sliding mode control (SMC), high-order sliding mode observer (HSMO), permanent magnet synchronous machine (PMSM).

I. INTRODUCTION

PERMANENT magnet synchronous machine (PMSM) and its digital drive system have been widely used in industrial applications, such as electric vehicles (EVs), e.g., Toyota Prius, Chevy Volt and Nissan Leaf [1]. This is mainly due to its superior features, i.e., high power density, high efficiency, precise performance, high torque-current ratio and compact structure [1]–[3].

To achieve good drive performance, field oriented control (FOC), with low torque ripple, fast dynamic response and high

Manuscript received March 15, 2017; revised July 16, 2017; accepted September 7, 2017. Date of publication September 15, 2017; date of current version January 15, 2018. This work was supported by the National Natural Science Foundation under Grant 51377065 and Grant 61773284. The review of this paper was coordinated by the Guest Editors of the VPPC 2016 Special Section. (Corresponding author: Wei Xu.)

Y. Jiang, W. Xu, and Y. Liu are with the State Key Laboratory of Advanced Electromagnetic Engineering and Technology, School of Electrical and Electronic Engineering, Huazhong University of Science and Technology, Wuhan 430073, China (e-mail: yajiejiang@foxmail.com; weixu@hust.edu.cn; liuyi82@hust.edu.cn).

C. Mu is with the School of Electrical and Information Engineering, Tianjin University, Tianjin 300072, China (e-mail: cxmu@tju.edu.cn).

Color versions of one or more of the figures in this paper are available online at <http://ieeexplore.ieee.org>.

Digital Object Identifier 10.1109/TVT.2017.2752778

control precision, has been the universal control strategy of PMSM in EVs. In a typical double-loop structure based FOC strategy, the outer speed loop influences the speed and torque response, and the inner current loop decides the dynamic and steady performance of the whole drive system.

The designing of speed loop should achieve good speed tracking performance and anti-external disturbance capability. Apart from classical proportional-integral (PI) control, till now, many advanced control methods have been applied in the speed loop, such as fuzzy control [4], adaptive control [5], [6], sliding mode control (SMC) [7], [8], etc. Among these methods, SMC with invariance is one popular strategy for non-linear systems with external disturbances, and can get fast dynamic response and strong robustness [9]. As applied to the speed loop, SMC can help improve the speed tracking accuracy and torque dynamic performance of PMSM drive system. However, in order to restrain the disturbances like varying load torque, large switching gain is generally introduced in the traditional SMC method, leading to discontinuous control signal and serious chattering with high frequency oscillation.

As for the current loop, to obtain precise steady-state control and fast dynamic current/torque response, different algorithms have been studied, e.g., hysteresis control, PI control, and predictive current control. However, the variable switching frequency and large current ripple resulted from hysteresis control cannot be avoided. Meanwhile, the linear PI control with fixed switching frequency is not able to achieve ideal dynamic and stable performance in the nonlinear PMSM drive system with parameter uncertainties and external disturbances. Theoretically, the predictive current control contains, model predictive control (MPC) [10], [11], and deadbeat-based predictive current control (DPCC) [12]–[21]. Based on discrete models of PMSM, the MPC can forecast and determine the future voltage vector to achieve the optimization of cost function. In this way, strong robustness can be obtained by MPC. However, precise prediction needs high computational efforts and extra hardware requirements, which greatly limit the industrial application of MPC. In contrary to the MPC, the DPCC based discrete model calculates the required preset voltages in every sampling period, and translates them into switching signals through pulse-width modulation (PWM) technology. In this way, the DPCC is characterized with fixed switching frequency, good static current tracking accuracy, fast current dynamic response, and less

computational burden. Therefore, the DPCC has been adopted in many industrial fields, e.g., inverter control, and machine drives [12].

It is well known that the conventional DPCC completely depends on a given model, resulting in control performance deterioration when faced with parameter mismatches and unmodeled system dynamics, which cannot be effectively avoided in practical applications. Specially, for PMSM drive system of EVs, the ambient temperature, magnetic saturation, and load conditions vary quite violently under various working environment [15]–[17], which would bring significant influence to machine parameters and vehicle inertia. To solve the fore-mentioned drawbacks, some methods have been proposed to improve the performance of DPCC. In [11] and [18], one luenberger observer is presented to compensate DPCC for the prediction delay and machine parameter deviation. In [19], a discrete-time integral term is added to DPCC to overcome parametric uncertainties and unmodeled dynamics. In [20], weight modification algorithm is proposed to enhance the robustness of DPCC. In [21], a discrete filter is developed for the parameter variety compensation of inverter.

Among disturbance observation techniques, the sliding mode observer (SMO) with high robustness has been used for disturbance observation and compensation system uncertainties. [7]. Meanwhile, compared with the conventional first-order sliding mode disturbance observer, high-order sliding mode observer (HSMO) has advantages of chattering suppression and excellent dynamic performance. The HSMO has also been used for disturbance estimation in many industrial applications, especially in machine and mechanical drive systems [22]. Therefore, to solve the afore-mentioned problems of speed and current loops in PMSM drive system, one HSMO is employed in this paper to provide precise estimation and compensation for the external disturbance and parameter mismatches.

One DPCC scheme based sliding mode for PMSM drive system is studied in this paper. Firstly, the parameter variation and external disturbance of PMSM model are analyzed. Then, a novel PMSM model, which contains an ideal part with nominal parameters and a disturbance part of parameters mismatch and external disturbances, is derived. Based on the ideal mode part, a sliding mode speed controller is designed for the speed loop, and a discrete DPCC is proposed for the current regulation. Meanwhile, a unified HSMO is designed for the estimation of disturbances and uncertainties in speed, d - and q - current loops. Furthermore, the estimated values are used as the feedback compensation of the proposed SMC and DPCC. Thus, the proposed control strategy can achieve fast dynamic response and precise steady-state performance for a PMSM drive system with acute variations of load or parameters. Lastly, the control algorithm is verified by comprehensive experiments.

The structure of this paper is organized as follows. In Section II, one novel PMSM system model is built up, together with the design of sliding mode speed controller and DPCC. Then the HSMO and its stability analysis are provided in Section III. In Section IV, relative analyses of the improved drive system are given. Experimental results are presented in Section V. And finally, the conclusions are drawn in Section VI.

II. PMSM MODEL AND CONTROL ALGORITHMS

A. Modeling of PMSM With Uncertainties and Disturbances

The current and motion equations of PMSM in synchronous rotating frame can be described as [8]

$$\begin{aligned}\dot{i}_d &= -\frac{R_s}{L}i_d + \omega_e i_q + \frac{1}{L}u_d \\ \dot{i}_q &= -\omega_e i_d - \frac{R_s}{L}i_q + \frac{1}{L}u_q - \frac{1}{L}\omega_e \psi_f \\ \dot{\omega}_e &= \frac{3}{2} \frac{n_p^2}{J} \psi_f i_q - \frac{B}{J}\omega_e - \frac{n_p}{J}T_L\end{aligned}\quad (1)$$

where u_d and u_q are the d - and q - axes stator voltages, i_d and i_q the d - and q - axes stator currents, L_d and L_q the d - and q -axes stator inductances, R_s the stator resistance, ω_e the rotor electrical angular velocity, n_p the number of pole pairs, ψ_f the flux linkage, T_L the load torque, B the viscous damping coefficient, and J the moment of inertia.

In this paper, considering parameter variations, the PMSM model can be reformed into a general form

$$\begin{aligned}\frac{d}{dt} \begin{bmatrix} i_d \\ i_q \end{bmatrix} &= \begin{bmatrix} -\frac{R_{s0}}{L_0} & \omega_e \\ -\omega_e & -\frac{R_{s0}}{L_0} \end{bmatrix} \begin{bmatrix} i_d \\ i_q \end{bmatrix} + \begin{bmatrix} \frac{1}{L_0} & 0 \\ 0 & \frac{1}{L_0} \end{bmatrix} \begin{bmatrix} u_d \\ u_q \end{bmatrix} + \begin{bmatrix} 0 \\ -\frac{\omega_e \psi_{f0}}{L_0} \end{bmatrix} \\ &\quad + \begin{bmatrix} -\frac{\Delta L}{L_0} \dot{i}_d - \frac{\Delta R_s}{L_0} i_d + \frac{\Delta L}{L_0} \omega_e i_q \\ -\frac{\Delta L}{L_0} \dot{i}_q - \frac{\Delta L}{L_0} \omega_e i_d - \frac{\Delta R_s}{L_0} i_q + \frac{\Delta \psi_f}{L_0} \omega_e \end{bmatrix}\end{aligned}\quad (2)$$

$$\dot{\omega}_e = \frac{3}{2} \frac{n_p^2}{J_0} \psi_{f0} i_q - \frac{B}{J_0} \omega_e - \frac{n_p}{J_0} T_L - \frac{\Delta J}{J_0} \dot{\omega}_e + \frac{3}{2} \frac{n_p^2}{J_0} \Delta \psi_f i_q \quad (3)$$

where R_{s0} , L_0 and ψ_{f0} are the fixed nominal parameters of the PMSM, ΔR_s , ΔL and $\Delta \psi_f$ are the parameters variations, and the actual values of these parameters are $R_s = R_{s0} + \Delta R_s$, $L = L_0 + \Delta L$, $\psi_f = \psi_{f0} + \Delta \psi_f$, and $J = J_0 + \Delta J$. According to (2) and (3), the current and motion equations of PMSM can be expressed in matrix form

$$\frac{d}{dt} \mathbf{i} = \mathbf{A}_0 \cdot \mathbf{i} + \mathbf{B}_0 \cdot \mathbf{u} + \mathbf{C}_0 + \mathbf{d}_{dq} \quad (4)$$

$$\frac{d\omega_e}{dt} = \frac{3}{2} \frac{n_p^2}{J_0} \psi_{f0} i_q - \frac{B}{J_0} \omega_e + d_\omega(t) \quad (5)$$

where $\mathbf{A}_0 = \begin{bmatrix} -\frac{R_{s0}}{L_0} & \omega_e \\ -\omega_e & -\frac{R_{s0}}{L_0} \end{bmatrix}$, $\mathbf{B}_0 = \begin{bmatrix} \frac{1}{L_0} & 0 \\ 0 & \frac{1}{L_0} \end{bmatrix}$, $\mathbf{C}_0 = \begin{bmatrix} 0 \\ -\frac{\omega_e \psi_{f0}}{L_0} \end{bmatrix}$, $\mathbf{d}_{dq} = \begin{bmatrix} d_d(t) \\ d_q(t) \end{bmatrix} = \begin{bmatrix} -\frac{\Delta L}{L_0} \dot{i}_d - \frac{\Delta R_s}{L_0} i_d + \frac{\Delta L}{L_0} \omega_e i_q \\ -\frac{\Delta L}{L_0} \dot{i}_q - \frac{\Delta L}{L_0} \omega_e i_d - \frac{\Delta R_s}{L_0} i_q + \frac{\Delta \psi_f}{L_0} \omega_e \end{bmatrix}$, and $d_\omega(t) = -\frac{n_p}{J_0} T_L - \frac{\Delta J}{J_0} \dot{\omega}_e + \frac{3}{2} \frac{n_p^2}{J_0} \Delta \psi_f i_q$. \mathbf{d}_{dq} is the total impacts of parameter mismatches and converter nonlinearity in the current loops, and $d_\omega(t)$ stands for the total impacts of parameter mismatches and external disturbance in the speed loop.

B. Design and Analysis of Sliding Mode Speed Controller

In order to achieve fast speed response, a sliding mode speed controller is designed on basis of exponential reaching law.

The speed tracking error is defined as $e_\omega = \omega_e^* - \omega_e$, and sliding mode variable as $s = c \cdot e_\omega + \dot{e}_\omega$. The sliding mode speed controller has been proposed in [7], which can be written as

$$i_q^* = \frac{2J}{3n_p^2 \psi_f} \left\{ \dot{\omega}_e^* + c \cdot e_\omega + \int [\varepsilon \operatorname{sgn}(s) + k \cdot s] \right\} \quad (6)$$

where i_q^* is the controller output, ω_e^* and $\dot{\omega}_e^*$ are the given speed and its derivative, $c > 0$ is a positive constant of the sliding mode variable, $\varepsilon > 0$ and $k > 0$ are switching gain and exponent coefficient of reaching law. The selection of these coefficients will be analyzed in Section V.

Theorem 2.1.: ε should be proportional to the derivative of $d_\omega(t)$, and the speed controller can obtain robustness against $d_\omega(t)$. The proof has been proposed in Appendix A.

According to (5), it can be found that the variations of external load, inertia and flux linkage will affect the control performance. Considering these factors, the switching gain is usually required to be designed relatively large for obtaining fast response. As a result, the chattering occurs, which can be solved by HSMO in this paper.

C. Design and Analysis of Conventional DPCC

In this paper, DPCC is proposed to achieve fast current dynamic response and precise tracking. According to the PMSM model illustrated in (4), applying the first-order Taylor method, and the discrete current model of PMSM can be expressed in matrix form

$$\begin{aligned} \mathbf{i}^*(k+1) = & (\mathbf{I} + \mathbf{A}_0 T_s) \cdot \mathbf{i}(k) + \mathbf{B}_0 T_s \cdot \mathbf{u}(k) + \mathbf{C}_0 T_s \\ & + T_s \mathbf{d}_{dq}(k) \end{aligned} \quad (7)$$

where $\mathbf{i}^*(k+1)$ is the current command value, and T_s is the sampling period. Traditional DPCC according to the ideal discrete PMSM model, regardless of the model uncertainties and disturbances in both d - and q -axis. The traditional DPCC law is given by

$$\mathbf{u}(k) = \frac{\mathbf{i}^*(k+1) - \mathbf{i}(k)}{B_0 T_s} - \frac{\mathbf{A}_0}{B_0} \mathbf{i}(k) - \frac{\mathbf{C}_0}{B_0} \quad (8)$$

According to (8), it is obvious that DPCC is a kind of model-based approaches. And the predictive model contains three parameters, stator inductance, stator resistance and permanent magnetic flux linkage, whose accuracies determinate the control performance of DPCC. Therefore, parameter sensitivity analysis is conducted in this section. Combining the model (7) and predictive control law (8), it obtains

$$\mathbf{i}(k+1) = \mathbf{i}^*(k+1) + T_s \mathbf{d}_{dq}(k) \quad (9)$$

The relations between the d - and q - current commands and their responses under parameter variations as described in (9). The parameter mismatches and nonlinearity would seriously deteriorate the control performance, which can be regarded as the disturbances in the current loops. Therefore, the DPCC should be promoted by more effective methods,

e.g., sliding mode disturbance observer developed in the next section.

III. ESTIMATION OF DISTURBANCE AND UNCERTAINTIES

From what has been analyzed above, conventional SMC and DPCC cannot guarantee the ideal performance of PMSM drive system. Therefore, observer based disturbance estimation method is applied to estimate the uncertainties and disturbances of speed and current loops in PMSM drive system. However, the conventional observer has limitation of current estimation, e.g., Luenberger observer generates steady-state errors, chattering occurs in the first-order SMO, etc. High-order sliding mode differentiator was designed by Levant in 2003 [18], and has been used for numerical calculation. In this paper, it can be transformed to be a high-order sliding-mode disturbance observer, and the design process is as follows. Considering a universal system, e.g., $\dot{x} = f(x) + d(t)$, where x is the states, $f(x)$ is the model function, and $d(t)$ is the system disturbance. And its high-order sliding-mode disturbance observer can be designed as

$$\begin{cases} \dot{z}_0 = v_0 + f(x) \\ v_0 = -\eta_0 K^{\frac{1}{3}} |z_0 - x|^{\frac{2}{3}} \operatorname{sgn}(z_0 - x) + z_1 \\ \dot{z}_1 = v_1, \\ v_1 = -\eta_1 K^{\frac{1}{2}} |z_1 - v_0|^{\frac{1}{2}} \operatorname{sgn}(z_1 - v_0) + z_2 \\ \dot{z}_2 = -\eta_2 K \operatorname{sgn}(z_2 - v_1) \end{cases} \quad (10)$$

where η_0 , η_1 , η_2 and K are the observer coefficients, z_0 , z_1 , z_2 the observe variables, v_0 and v_1 the intermediate variables. Thus, z_1 can converge to disturbance $d(t)$ in infinite time with appropriate parameter selections. The detailed descriptions of HSMO used for the speed and current loops are given in the sub-sections.

A. Observer Design of Speed Loop

Based on the modified PMSM motion (5), the HSMO of speed loop is designed as

$$\begin{cases} \hat{\omega}_e = \frac{3}{2} \frac{n_p^2}{J_0} \psi_{f0} i_q - \frac{B}{J_0} \hat{\omega}_e + v_{\omega 0} \\ v_{\omega 0} = -\eta_0 K^{\frac{1}{3}} |\hat{\omega}_e - \omega_e|^{\frac{2}{3}} \operatorname{sgn}(\hat{\omega}_e - \omega_e) + \hat{d}_\omega \\ \dot{\hat{d}}_\omega = v_{\omega 1} \\ v_{\omega 1} = -\eta_1 K^{\frac{1}{2}} |\hat{d}_\omega - v_{\omega 0}|^{\frac{1}{2}} \operatorname{sgn}(\hat{d}_\omega - v_{\omega 0}) + z_\omega \\ \dot{z}_\omega = -\eta_2 K \operatorname{sgn}(z_\omega - v_{\omega 1}) \end{cases} \quad (11)$$

where $\hat{\omega}_e$, \hat{d}_ω and z_ω are the estimated speed, disturbance of speed loop and its derivative, $v_{\omega 0}$ and $v_{\omega 1}$ are intermediate variables, η_0 , η_1 , η_2 and K are coefficients whose values will be analyzed in Section III-C.

Applying the first-order Taylor method, and the discrete-time form of (11) is given as

$$\begin{cases} \hat{\omega}_e(k+1) = (1 - \frac{B}{J_0} T_s) \hat{\omega}_e(k) + \frac{3}{2} \frac{n_p^2}{J_0} \psi_{f0} T_s i_q(k) + T_s v_{\omega 0}(k) \\ v_{\omega 0}(k) = -\eta_0 K^{\frac{1}{3}} |\hat{\omega}_e(k) - \omega_e(k)|^{\frac{2}{3}} \operatorname{sgn}(\hat{\omega}_e(k) - \omega_e(k)) \\ \quad + \hat{d}_{\omega}(k) \\ \hat{d}_{\omega}(k) = \hat{d}_{\omega}(k-1) + T_s v_{\omega 1}(k-1) \\ v_{\omega 1}(k-1) = -\eta_1 K^{\frac{1}{2}} |\hat{d}_{\omega}(k-1) - v_{\omega 0}(k-1)|^{\frac{1}{2}} \operatorname{sgn}(\hat{d}_{\omega}(k-1) - v_{\omega 0}(k-1)) + z_{\omega}(k-1) \\ z_{\omega}(k-1) = z_{\omega}(k-2) - \eta_2 K T_s \operatorname{sgn}(z_{\omega}(k-2) - v_{\omega 1}(k-2)) \end{cases} \quad (12)$$

B. Observer Design of Current Loops

Based on the modified PMSM current (4), the HSMO of current loops are designed as

$$\begin{cases} \frac{d}{dt} \hat{\mathbf{i}} = \mathbf{A}_0 \cdot \mathbf{i} + \mathbf{B}_0 \cdot \mathbf{u} + \mathbf{C}_0 + \mathbf{v}_{i0} \\ \mathbf{v}_{i0} = -\eta_0 K^{\frac{1}{3}} |\hat{\mathbf{i}} - \mathbf{i}|^{\frac{2}{3}} \operatorname{sgn}(\hat{\mathbf{i}} - \mathbf{i}) + \hat{\mathbf{d}}_{dq} \\ \frac{d}{dt} \hat{\mathbf{d}}_{dq} = \mathbf{v}_{i1} \\ \mathbf{v}_{i1} = -\eta_1 K^{\frac{1}{2}} |\hat{\mathbf{d}}_{dq} - \mathbf{v}_{i1}|^{\frac{1}{2}} \operatorname{sgn}(\hat{\mathbf{d}}_{dq} - \mathbf{v}_{i1}) + \mathbf{z}_i \\ \frac{d}{dt} \mathbf{z}_i = -\eta_2 K \operatorname{sgn}(\mathbf{z}_i - \mathbf{v}_{i1}) \end{cases} \quad (13)$$

where $\hat{\mathbf{i}}$, $\hat{\mathbf{d}}_{dq}$ and \mathbf{z}_i are the estimated currents, disturbances of speed currents loop and its derivatives in d - and q -axis respectively, \mathbf{v}_{i0} and \mathbf{v}_{i1} are intermediate variables, η_0 , η_1 , η_2 and K are coefficients mentioned above.

Similarly, the discrete-time form of (13) is given as

$$\begin{cases} \hat{\mathbf{i}}(k+1) = (1 + \mathbf{A}_0 T_s) \hat{\mathbf{i}}(k) + \mathbf{B}_0 T_s \mathbf{u}(k-1) + \mathbf{C}_0 T_s \\ \quad + T_s \mathbf{v}_{i0}(k) \\ \mathbf{v}_{i0}(k) = -\eta_0 K^{\frac{1}{3}} |\hat{\mathbf{i}}(k) - \mathbf{i}(k)|^{\frac{2}{3}} \operatorname{sgn}(\hat{\mathbf{i}}(k) - \mathbf{i}(k)) + \hat{\mathbf{d}}_{dq}(k) \\ \hat{\mathbf{d}}_{dq}(k) = \hat{\mathbf{d}}_{dq}(k-1) + T_s \mathbf{v}_{i1}(k-1) \\ \mathbf{v}_{i1}(k-1) = -\eta_1 K^{\frac{1}{2}} |\hat{\mathbf{d}}_{dq}(k-1) - \mathbf{v}_{i0}(k-1)|^{\frac{1}{2}} \\ \quad \times \operatorname{sgn}(\hat{\mathbf{d}}_{dq}(k-1) - \mathbf{v}_{i0}(k-1)) + \mathbf{z}_i(k-1) \\ \mathbf{z}_i(k-1) = \mathbf{z}_i(k-2) - \eta_2 K T_s \operatorname{sgn}(\mathbf{z}_i(k-2) - \mathbf{v}_{i1}(k-2)) \end{cases} \quad (14)$$

To demonstrate the superior performance of HSMO, the simulation results of currents estimation on basis of SMO, Luenberger observer and HSMO are shown in Fig. 1. From the picture, it is obvious that the HSMO excels at perfect current observation. Corresponding to the analysis, large chattering occurs in the first-order SMO, and steady-error deteriorates the observe performance of Luenberger observer.

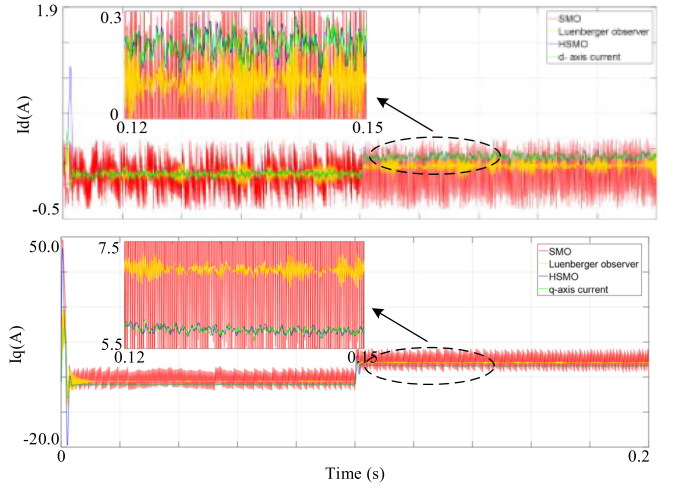


Fig. 1. Simulation of d - and q -axis current observation.

C. Observer Stability Analysis

Taking the HSMO of speed loop (11) as example, the stability analysis of HSMO is proposed in this section. It is assumed that the differentiable inputs of HSMO, ω_e and i_q have Lipschitz constant $M > 0$ for its derivatives. Then, the error variables of HSMO are defined as $\varepsilon_0 = \hat{\omega}_e - \omega_e$, $\varepsilon_1 = \hat{d}_{\omega} - d_{\omega}$, and $\varepsilon_2 = \hat{d}_{\omega} - \dot{d}_{\omega}$. Combining (5) and (11), the observer error dynamics can be given by

$$\begin{cases} \dot{\varepsilon}_0 = -\frac{B}{J} (\varepsilon_0) - \eta_0 K^{\frac{1}{3}} |\varepsilon_0|^{\frac{2}{3}} \operatorname{sgn}(\varepsilon_0) + \varepsilon_1 \\ \dot{\varepsilon}_1 = -\eta_1 K^{\frac{1}{2}} |\varepsilon_1 - \dot{\varepsilon}_0|^{\frac{1}{2}} \operatorname{sgn}(\varepsilon_1 - \dot{\varepsilon}_0) + \varepsilon_2 \\ \dot{\varepsilon}_2 \in -\eta_2 K \operatorname{sgn}(\varepsilon_2 - \dot{\varepsilon}_1) + [-M, M] \end{cases} \quad (15)$$

In order to analyze the HSMO stability, the Lyapunov functions and their satisfy conditions are expressed as

$$\begin{cases} V_1 = \varepsilon_0^2, \dot{V}_1 = \varepsilon_0 \cdot \dot{\varepsilon}_0 \leq 0 \\ V_2 = \varepsilon_1^2, \dot{V}_2 = \varepsilon_1 \cdot \dot{\varepsilon}_1 \leq 0 \\ V_3 = \varepsilon_2^2, \dot{V}_3 = \varepsilon_2 \cdot \dot{\varepsilon}_2 \leq 0 \end{cases} \quad (16)$$

According to the principles of HSMO, the convergence of observer variables are $\hat{\omega}_e \rightarrow \omega_e$, $\hat{d}_{\omega} \rightarrow d_{\omega}$, and $\mathbf{z}_i = \hat{d}_{\omega} - \dot{d}_{\omega}$. Take the derivative of first Lyapunov function as

$$\begin{aligned} \dot{V}_1 &= \varepsilon_0 \cdot \dot{\varepsilon}_0 = \varepsilon_0 \cdot \left(-\frac{B}{J} (\varepsilon_0) - \eta_0 K^{\frac{1}{3}} |\varepsilon_0|^{\frac{2}{3}} \operatorname{sgn}(\varepsilon_0) + \varepsilon_1 \right) \\ &= -\frac{B}{J} (\varepsilon_0)^2 - \eta_0 K^{\frac{1}{3}} |\varepsilon_0|^{\frac{5}{3}} + \varepsilon_0 \cdot \varepsilon_1 \end{aligned} \quad (17)$$

It can be concluded that in such condition, $\dot{V}_1 \leq 0$ can be satisfied with proper choices of the parameters η_0 and K . Meanwhile, $\dot{\varepsilon}_0$ will converge to ε_1 . Combining the error dynamics (15), it is perspicuous that the two other errors can be described

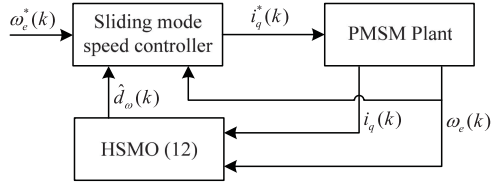


Fig. 2. Diagram of sliding mode speed control with HSMO.

as the functions of speed observation error:

$$\begin{aligned} \varepsilon_1 - \dot{\varepsilon}_0 &= \frac{B}{J}(\varepsilon_0) + \eta_0 K^{\frac{1}{3}} |\varepsilon_0|^{\frac{2}{3}} \operatorname{sgn}(\varepsilon_0) \\ \varepsilon_2 - \dot{\varepsilon}_1 &= \eta_1 K^{\frac{1}{2}} |\varepsilon_1 - \dot{\varepsilon}_0|^{\frac{1}{2}} \operatorname{sgn}(\varepsilon_1 - \dot{\varepsilon}_0) \\ &= \eta_1 K^{\frac{1}{2}} \left| \frac{B}{J}(\varepsilon_0) + \eta_0 K^{\frac{1}{3}} |\varepsilon_0|^{\frac{2}{3}} \operatorname{sgn}(\varepsilon_0) \right|^{\frac{1}{2}} \operatorname{sgn}\left(\frac{B}{J}(\varepsilon_0)\right) \\ &\quad + \eta_0 K^{\frac{1}{3}} |\varepsilon_0|^{\frac{2}{3}} \operatorname{sgn}(\varepsilon_0) \end{aligned} \quad (18)$$

Similar to the afore analysis of V_1 , $\dot{V}_2 \leq 0$ and $\dot{V}_3 \leq 0$ can be satisfied with proper choice of the parameter η_1 , η_2 and K . As a summary, in order to meet the demand of (16), it is obtained

$$\begin{aligned} \eta_0 K^{\frac{1}{3}} &\geq -\frac{B}{J} |\varepsilon_0|^{\frac{1}{3}} \pm \frac{\varepsilon_1}{\varepsilon_0^{\frac{3}{2}}} \\ \eta_1 K^{\frac{1}{2}} &\geq \max \left(\frac{\varepsilon_2}{|\varepsilon_0|^{\frac{1}{2}}} \right) \\ \eta_2 K &\geq M \end{aligned} \quad (19)$$

The stability analysis of HSMO is finished here. And the specific parameters are given in Section V.

IV. DRIVE SYSTEM ANALYSIS

A. Speed Loop

First, he estimated external load and parameter mismatch of speed loop are compensated to the sliding mode speed controller with feedback, which can be written as

$$u = \frac{2J}{3n_p^2 \psi_f} \left\{ \dot{\omega}_e^* + ce_\omega - \frac{J}{n_p} \hat{d}_\omega(t) + \int [\varepsilon \operatorname{sgn}(s) + k \cdot s] \right\} \quad (20)$$

Thus, the dynamic performance, load robustness of speed loop is significantly improved. Meanwhile, since the switching gain ε can be selected relatively small, the chattering of speed and torque are reduced. Ignoring current loops, the speed control scheme is described in Fig. 2.

Considering that machine electrical time constant is much smaller than the mechanical time constant, and that the sampling period T_s in Digital signal processor (DSP) is noticeably short, the time delay of speed loop can be ignored.

B. Current Loop

As an industrial control system, the data sampling, algorithm execution and PWM of PMSM drive system, cannot be finished

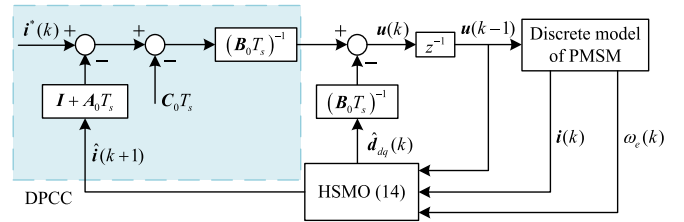


Fig. 3. Diagram of DPCC with HSMO.

in one interrupt period. Therefore, the time delay should be considered for accurate DPCC. In the universal DSP based PMSM platform, sampling is synchronizing with the PWM interrupt signals. Meanwhile, it can be concluded that the sampling and algorithm execution should be finished one sampling period ahead before PWM update [12]. Then, one sampling period time delay would exist in the estimated disturbance from the discrete-time model of HSMO (14). Lastly, (7) is modified as

$$\begin{aligned} \mathbf{i}(k+1) &= (\mathbf{I} + \mathbf{A}_0 T_s) \cdot \mathbf{i}(k) + \mathbf{C}_0 T_s + \mathbf{B}_0 T_s \cdot \mathbf{u}(k-1) \\ &\quad + T_s \hat{\mathbf{d}}_{dq}(k-1) \end{aligned} \quad (21)$$

Setting $\mathbf{i}(k+2) = \mathbf{i}^*(k)$, and the command voltages based traditional DPCC is given as

$$\mathbf{u}(k) = \frac{\mathbf{i}^*(k) - \mathbf{i}(k+1)}{B_0 T_s} - \frac{\mathbf{A}_0}{B_0} \mathbf{i}(k+1) - \frac{\mathbf{C}_0}{B_0} \quad (22)$$

At the same time, the estimated parameter mismatched disturbances, are feedbacked to conventional DPCC, which is written as

$$\mathbf{u}(k) = \frac{\mathbf{i}^*(k) - \hat{\mathbf{i}}(k+1)}{B_0 T_s} - \frac{\mathbf{A}_0}{B_0} \hat{\mathbf{i}}(k+1) - \frac{\mathbf{C}_0}{B_0} - \frac{\hat{\mathbf{d}}_{dq}(k)}{B_0} \quad (23)$$

Since the parameter mismatches are compensated, the dynamic performance, stability precision of current loops are improved significantly. Ignoring speed loop, the proposed discrete predictive current control scheme is described in Fig. 3.

C. Coefficients Selection of Closed Loop System

By virtue of the compensated disturbances of current loops, (23) can be seen as the ideal DPCC, which is written as

$$\begin{aligned} \begin{bmatrix} u_d(k) \\ u_q(k) \end{bmatrix} &= \begin{bmatrix} \frac{L}{T_s} \cdot (i_d^*(k) - \hat{i}_d(k+1)) + R_s \cdot \hat{i}_d(k+1) - L \cdot \omega_e(k) \\ \frac{L}{T_s} \cdot (i_q^*(k) - \hat{i}_q(k+1)) + R_s \cdot \hat{i}_q(k+1) \end{bmatrix} \\ &\quad + \begin{bmatrix} -L \cdot \omega_e(k) \cdot \hat{i}_q(k+1) \\ L \cdot \omega_e(k) \cdot \hat{i}_d(k+1) + \omega_e(k) \psi_f \end{bmatrix} \end{aligned} \quad (24)$$

From (24), it is obvious that the DPCC can be equivalent to the feedback proportional control, in which the proportional coefficient is L/T_s , and the rest of the control law as the coupling control part. Hence, the DPCC transform function is defined as $P(s) = L/T_s$.

Theorem 4.1.: Sliding mode speed controller (20) can be equivalent to a PI controller with invariability of SMC against

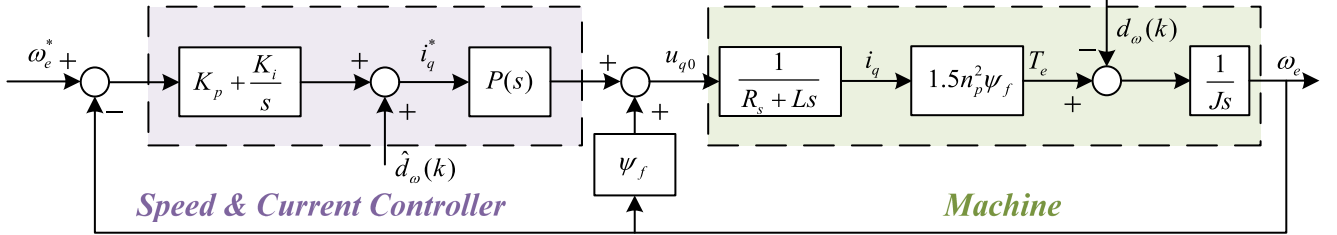


Fig. 4. Diagram of speed loop.

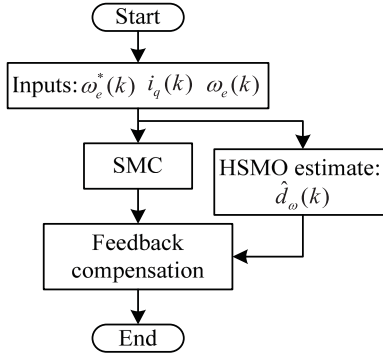


Fig. 5. Flow chart of speed loop.

disturbance and uncertainties, and the coefficients of PI are

$$K_p = 2J(c+k)/3n_p^2\psi_f, K_i = 2J \cdot c \cdot k / 3n_p^2\psi_f \quad (25)$$

The proof has been proposed in Appendix B.

Ignoring the viscous friction coefficient, the diagram of speed loop is shown in Fig. 4. Since the external disturbance and parameter mismatch are compensated, only the speed tracked response needs to be discussed in this section. According Fig. 4, the system transfer function is given as

$$\frac{\omega_e}{\omega_e^*} = \frac{1.5n_p^2\psi_f P(s)(K_p + K_i/s)}{Js(R_s + Ls) - 1.5n_p^2\psi_f^2 + 1.5n_p^2\psi_f P(s)(K_p + K_i/s)} \quad (26)$$

Therefore, the coefficients K_p and K_i can be selected on the light of the parameter selection principle of PI controller. Then, the values of c and k can be calculated based on (25), ε can be designed to obtain fast speed response. The proposed control flow chart of speed loop is shown in Fig. 5.

The proposed control flow chart of current loop is shown in Fig. 6.

As shown in Figs. 5 and 6, the whole DPCC based SMC strategy of PMSM drive system is proposed, which can not only keep the robustness under the condition of external load and parameter variations, but also improve the control precision of currents. The implementation process is summarized as follows

- 1) Measure the speed and q -axis current, input to HSMO (12), as well as estimating the equivalent current disturbance of speed loop, e.g., the load torque, and parameter mismatch. Then, the disturbance is compensated to the sliding mode speed controller, and the optimized q -axis reference current is produced.

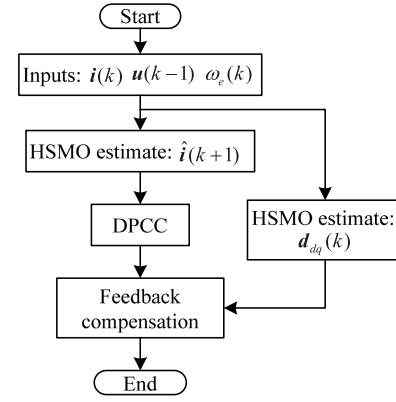


Fig. 6. Flow chart of current loop.

TABLE I
PARAMETERS OF PMSM

Symbol	Quantity	Value and Unit
Φ_f	Flux linkage of permanent magnet	0.35 Wb
n_p	Number of pole pairs	3
R_s	Stator phase resistance	0.8 Ω
B	Viscous friction coefficient	$1.74 * 10^{-5}$ N · ms/rad
L	d - and q - axis inductances	$5.0 * 10^{-3}$ H
J	Rotational inertia	$3.78 * 10^{-4}$ kg · m ²

- 2) Measure the d -axis current, together with q -axis current, speed and voltages input to HSMO (14). And the equivalent voltage disturbance in current loops is calculated, which is compensated to the predictive current control. Thus, the optimized command voltages are generated.
- 3) Command voltages are transferred to switching signals of switching devices with SVPWM module.
- 4) Phase voltages are generated, and used to drive PMSM.

V. EXPERIMENTS

To demonstrate the effectiveness of the proposed method, in this section, experiments based on one PMSM drive system are investigated in details. The parameters of the PMSM are listed in Table I.

The proposed control strategy is implemented in an experimental bench with TI TMS320F28335 DSP board, as shown in Figs. 7 and 8. A three-phase uncontrolled rectifier is applied to provide DC power, from which the three-phase PWM converter conducts alternating current for PMSM drive. The PMSM speed is conducted by a rotary transformer. The sampling frequency of speed loop is 1 kHz, and the counterpart of current loop is

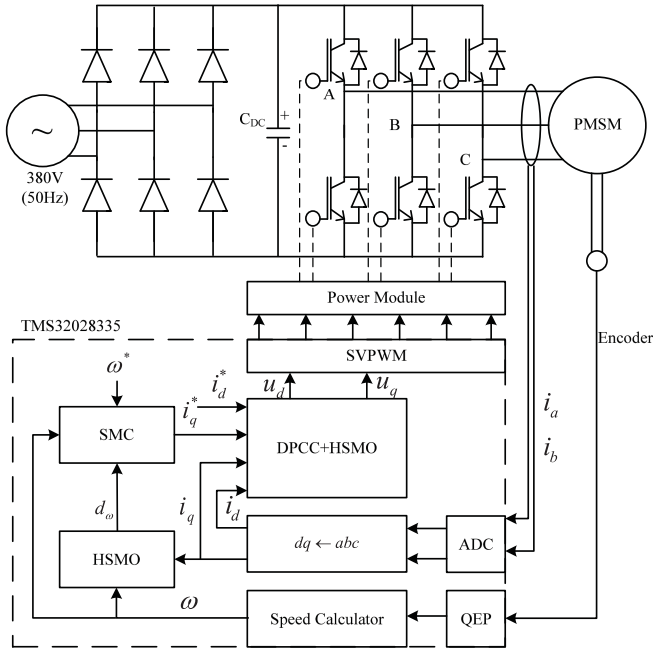


Fig. 7. Block diagram of the experimental bench.

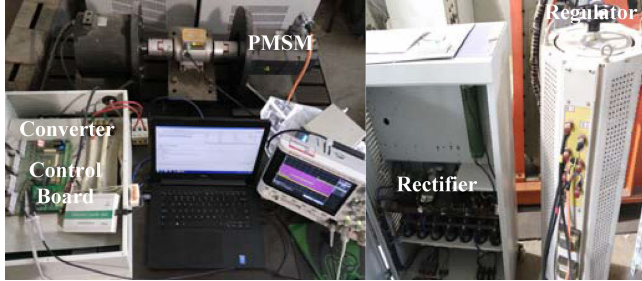


Fig. 8. PMSM drive platform.

5 kHz. Specially, the 200 μ s execution period can satisfy the computational burden of the proposed DPCC algorithm without additional hardware. Main drive indexes are outputted to digital oscilloscope through the D/A converter modules on the DSP board, except for stator phase currents that are measured by current probes. The control strategy contains one sliding mode controller and DPCC+HSMO structure. The PMSM drive platform is shown in Fig. 8.

According to the aforementioned analysis, the experiential coefficients are selected as follows: $c = 100.0$, $k = 20.0$, $\varepsilon = 5.0$ for speed controller, and $K = 1.0 \times 10^6$, $\eta_0 = 3.0$, $\eta_1 = 1.5$, $\eta_2 = 1.1$ for HSMO.

A. Performance Test

Firstly, the experimental results of speed increase are presented to test the system performance of the proposed scheme, as shown in Fig. 9, where the machine starts at 0.4 s and achieves rated speed within 0.5 s.

Secondly, the current responses of the proposed DPCC scheme and the conventional PI control are compared under the same conditions. Machine parameters used in the proposed

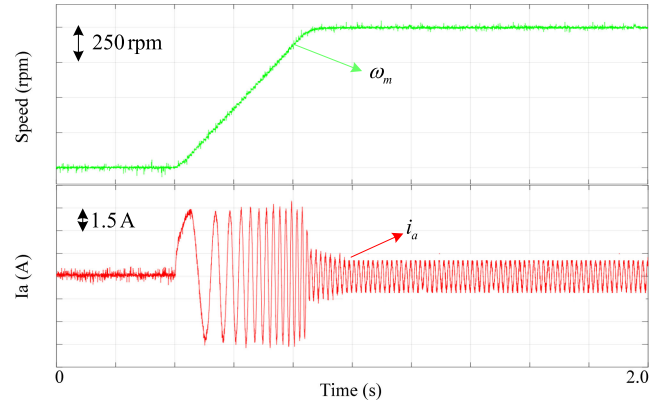


Fig. 9. Starting responses from standstill to 1000 rpm.

DPCC are rated, meanwhile the PI parameters in current-loop are tuned to optimal.

Fig. 10 shows the comparison of the two current controllers, with a step change of i_d^* from 0 to 6 A without load. The settling time of PI controller is obviously longer than that of the proposed controller, which means that the current dynamic performance of the proposed controller is faster than PI controller.

Fig. 11 shows the comparison of the two current controllers, with a step change of i_q^* from 1 to 7 A. Since the q -axis current is increased, the machine begins to speed up, which can be seen from the phase current responses. The q -axis current dynamic performance is similar to d -axis current response. The settling time of proposed controller is obviously shorter than the PI controller, which further illustrates the superiority of the proposed controller.

B. Speed-Loop Comparison Between Proposed SMC and PI

Fig. 12 shows the experimental results of the proposed SMC and conventional PI controllers to rated load respectively. Machine parameters of the controllers are rated values. In Fig. 12, speed fluctuation of PI controller is beyond 70 rpm, while that of the proposed DPCC is less than 50 rpm. Meanwhile, the recovery time of speed in proposed DPCC, is 0.4 s, which is much shorter than that of PI, 0.9 s. As analyzed in Section II, the estimated external disturbance can be calculated by the observed disturbance, $\hat{T}_L = -J_0 \cdot \hat{d}_\omega(t)/n_p$, as shown in Fig. 13.

Therefore, it is demonstrated that the proposed DPCC has better robustness against external disturbance in speed loop. Since the moment of inertia vary with the load, and has no effect on the external disturbance in steady-state, it is unnecessary to analyze its influence. Meanwhile, the flux mismatch is considered in current loop.

C. Current-Loop Comparison Between Proposed DPCC and Conventional DPCC

In order to evaluate the performance of proposed current control scheme under machine parameter mismatches, the experimental results of the proposed control scheme and conventional DPCC are shown in Figs. 14–21. The tests were done at 500 and 1000 rpm with 10 Nm load. The tested machine parameters

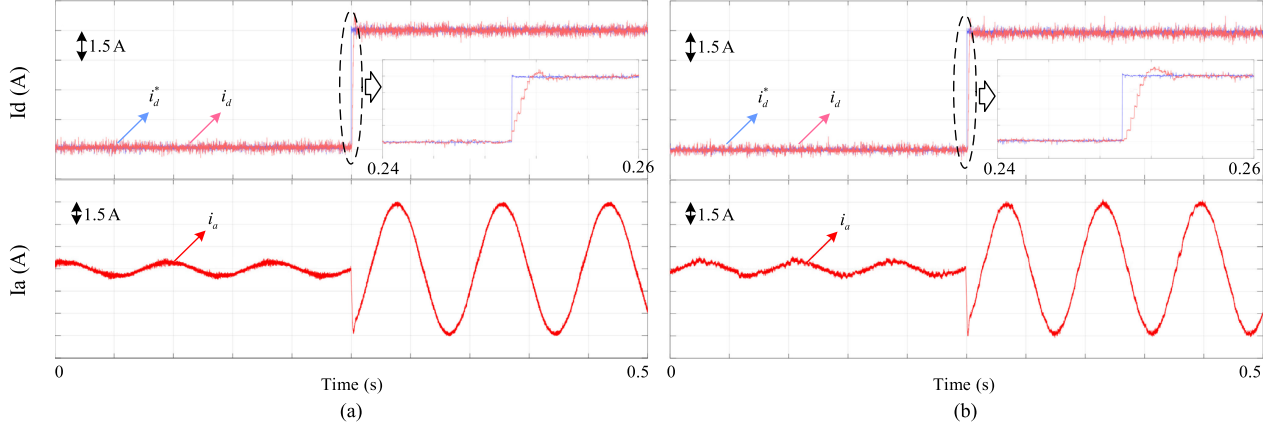


Fig. 10. Comparisons of the two controllers at step change of i_d in the amplitude from 0 to 6 A. (a) Proposed DPCC. (b) PI.

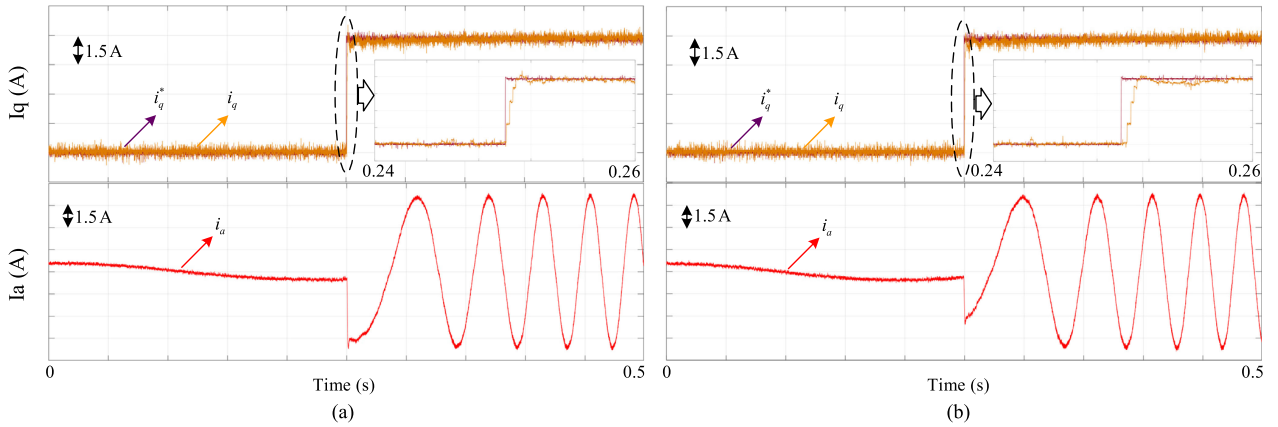


Fig. 11. Comparisons of the two controllers at step change of i_q in the amplitude from 1 to 7 A. (a) Proposed DPCC. (b) PI.

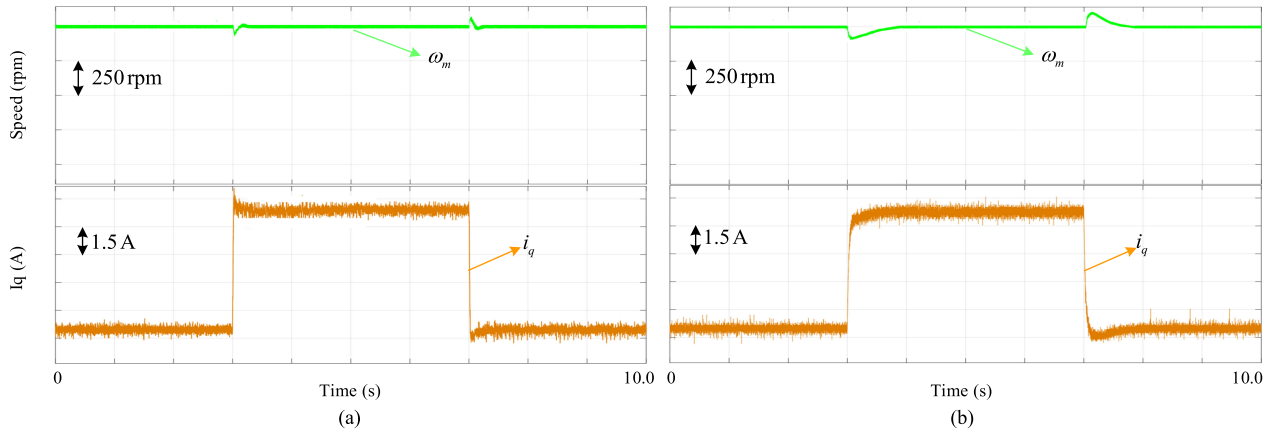


Fig. 12. Comparisons of the two controllers at step change of T_L in the amplitude from 0 to 10 Nm. (a) Proposed SMC. (b) PI.

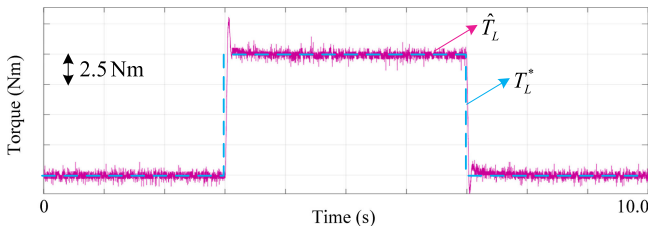


Fig. 13. Observation of load torque.

are selected as, inductance L , stator resistance R_s and permanent magnetic flux linkage ψ_f . Since the rated parameters of one machine cannot be changed freely, the sensitivities of three parameters are tested with changing their values in the DPCC, e.g., stator inductance of DPCC is set as $L_0 = 0.01$ H, while the real value is $L_0 = 0.005$ H, meaning that the stator inductance is reduced to half of its rated value. Meanwhile, the parameters are changing online with three steps in this paper. The presented results contain d- and q- axis currents i_d , i_q , and their refer-

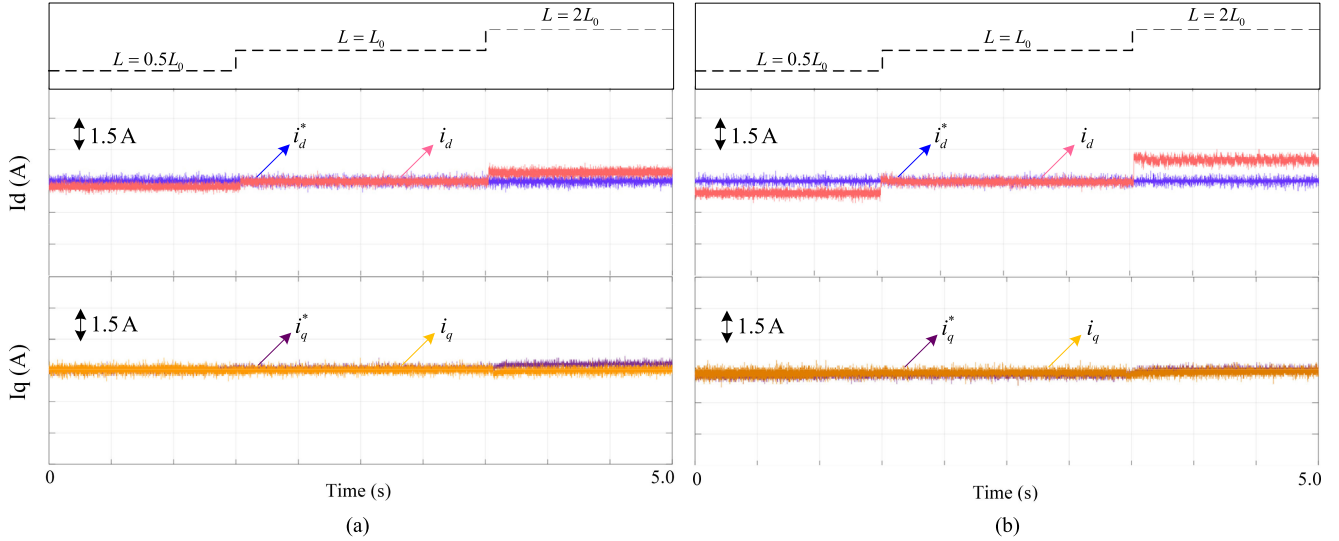


Fig. 14. Currents responses of conventional DPCC under inductance L mismatch. (a) 500 rpm 10 Nm. (b) 1000 rpm 10 Nm.

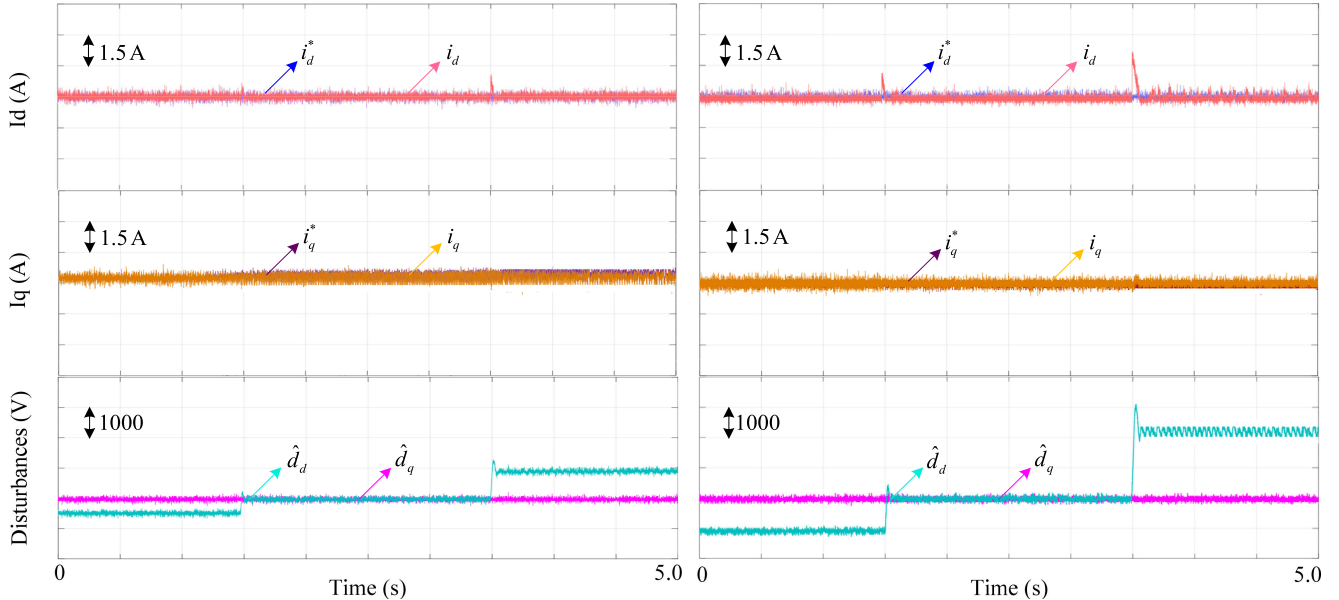


Fig. 15. Currents responses of the proposed DPCC under inductance L mismatch. (a) 500 rpm 10 Nm. (b) 1000 rpm 10 Nm.

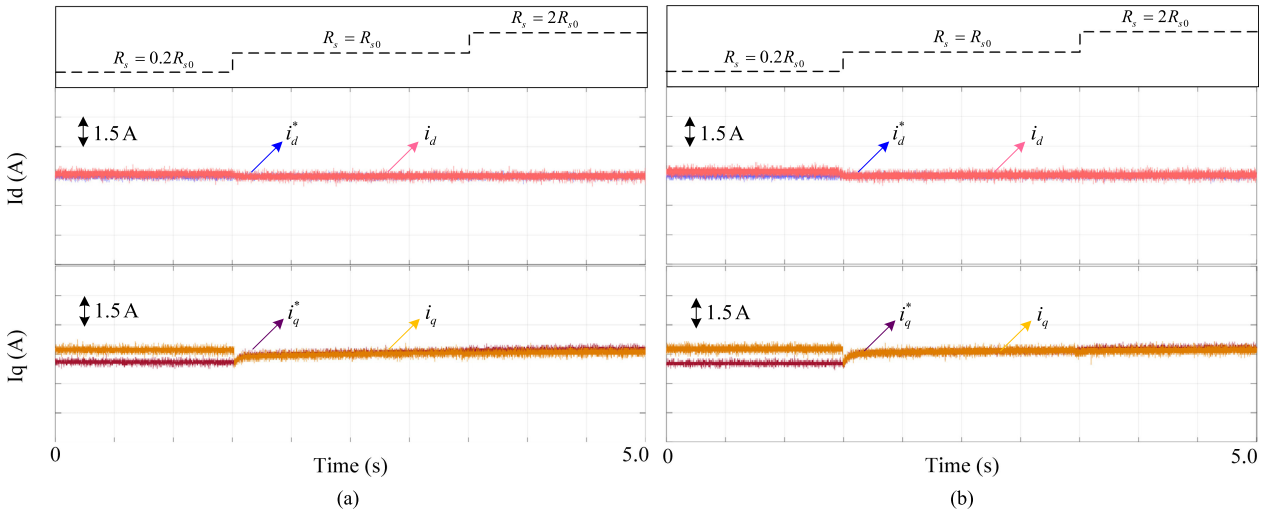


Fig. 16. Currents responses of conventional DPCC under resistance R_s mismatch. (a) 500 rpm 10 Nm. (b) 1000 rpm 10 Nm.

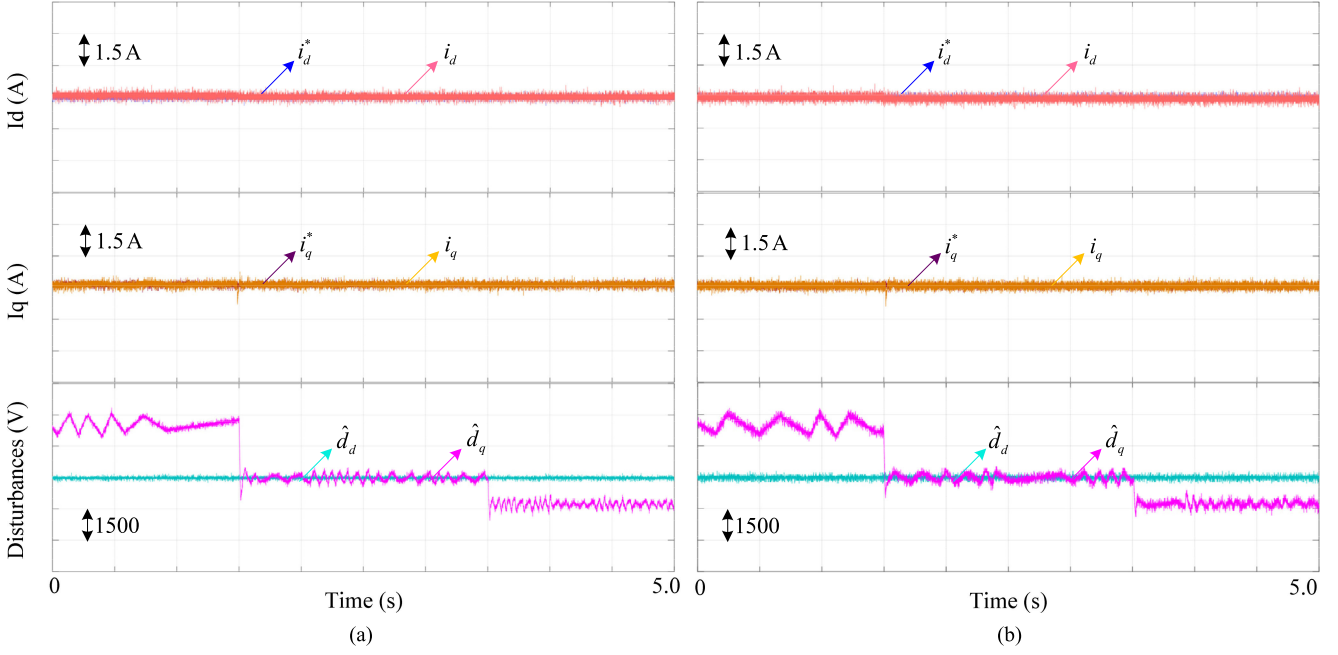


Fig. 17. Currents responses of the proposed DPCC under resistance R_s mismatch. (a) 500 rpm 10 Nm. (b) 1000 rpm 10 Nm.

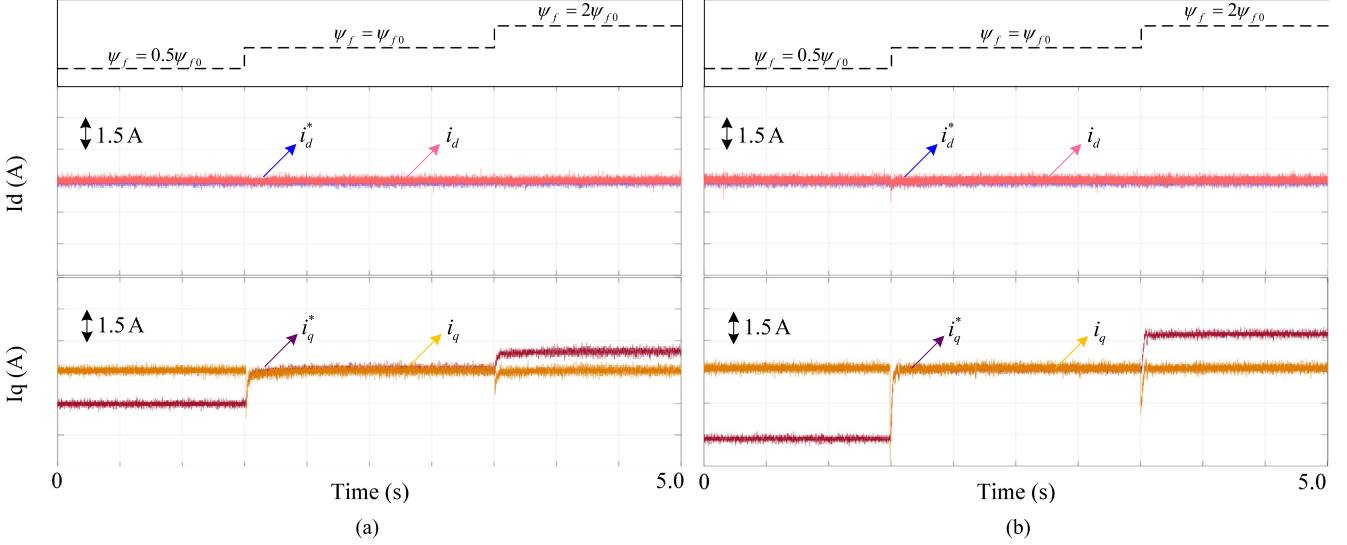


Fig. 18. Currents responses of conventional DPCC under flux ψ_f mismatch. (a) 500 rpm 10 Nm. (b) 1000 rpm 10 Nm.

ence values i_d^* , i_q^* . In addition, the estimated disturbances \hat{d}_d , \hat{d}_q equivalent to voltage disturbance, are also recorded in the results shown in Figs. 14–21.

Figs. 14 and 15 show the current response comparison of the conventional and proposed DPCC under inductance L mismatch, respectively. Change progress of inductance is $L = 0.5L_0 \rightarrow L_0 \rightarrow 2L_0$. Due to inductance mismatch, the real d-axis current of conventional DPCC cannot track the reference value accurately, as depicted in Fig. 14. And the current tracking error increases with the speed. Meanwhile, due to the coupling existed in PMSM model, the q-axis current is effected slightly. As for the proposed DPCC (Fig. 15), the disturbance caused by inductance mismatch is estimated by HSMO, and feedbacked to DPCC. Therefore, the steady-state current error is eliminated

effectively. Specially, according to the new model (4) in this paper, the inductance mismatch mainly generates d-axis disturbance. The estimated d- and q- axis disturbances are also given in the pictures.

Figs. 16 and 17 show the current response comparison of the conventional and proposed DPCC under stator resistance R_s mismatch respectively. Change progress of stator resistance is $R_s = 0.2R_{s0} \rightarrow R_{s0} \rightarrow 2R_{s0}$. Due to resistance mismatch, the real q-axis current cannot track the reference q-axis current accurately, illustrated in Fig. 16. According to the afore-analysis, the current tracking error increases with the load. Meanwhile, the d-axis current is deteriorated slightly. The resistance mismatch mainly generates q- axis disturbance, as shown in (4). As for the proposed DPCC (Fig. 17), the disturbance caused by

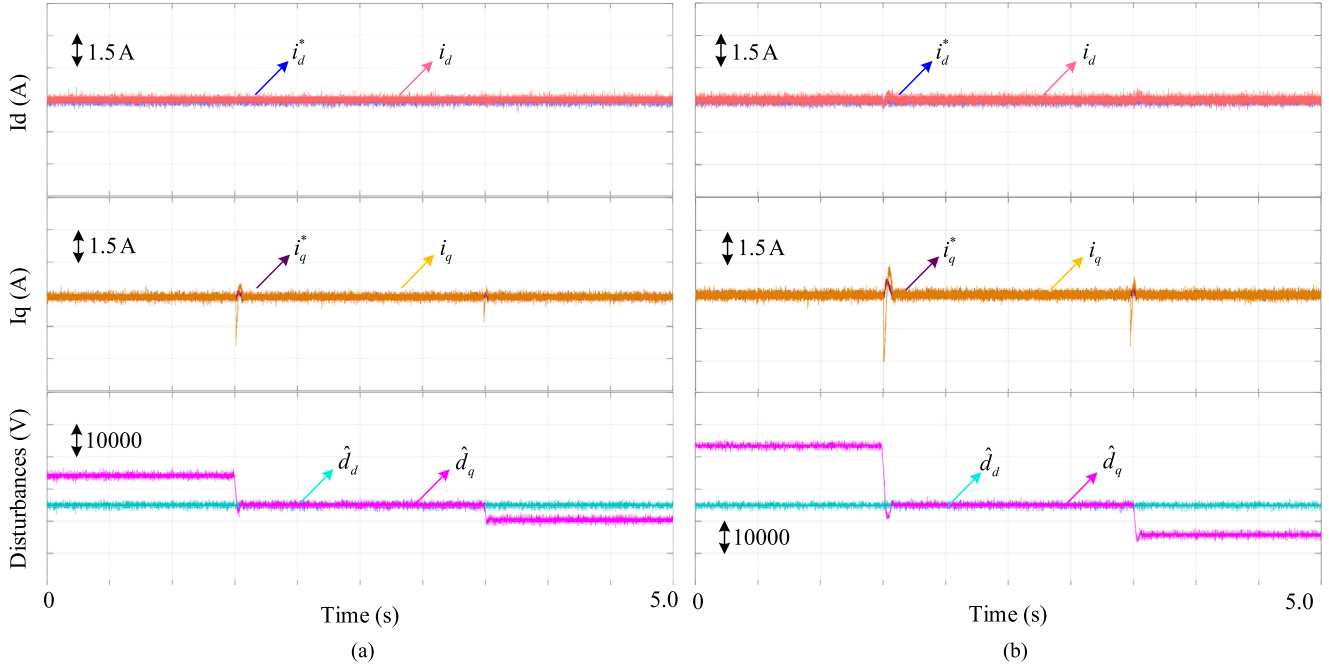


Fig. 19. Currents responses of the proposed DPCC under flux ψ_f mismatch. (a) 500 rpm 10 Nm. (b) 1000 rpm 10 Nm.

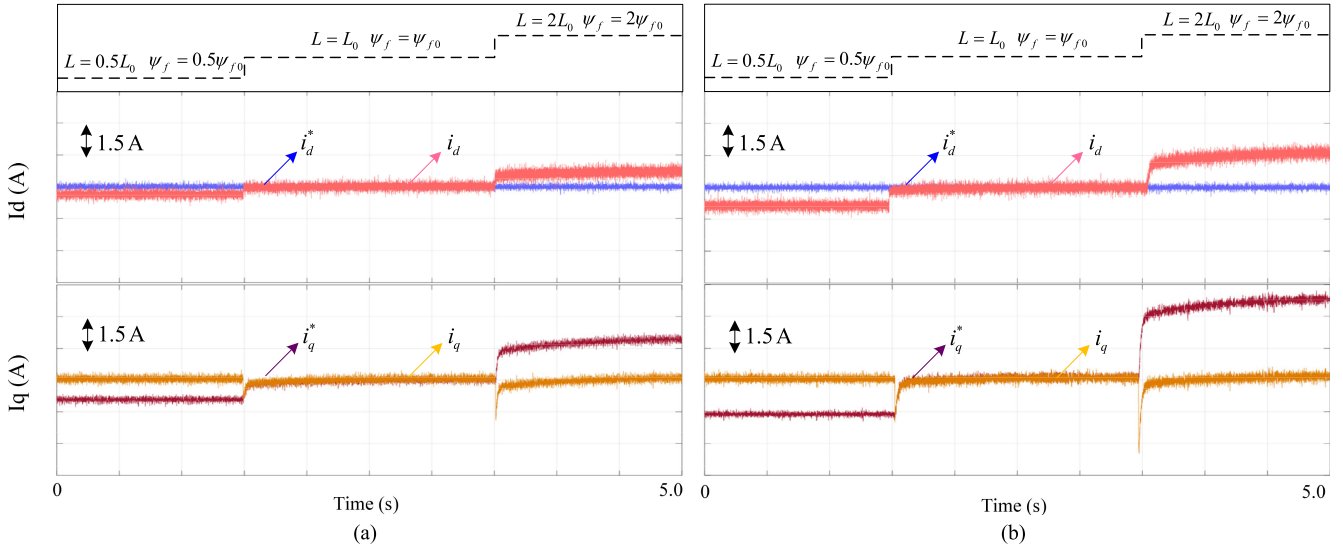


Fig. 20. Currents responses of conventional DPCC under inductance L and flux ψ_f mismatch. (a) 500 rpm 10 Nm. (b) 1000 rpm 10 Nm.

resistance mismatch is observed by HSMO, and feedback to DPCC. Therefore, the steady-state current error is eliminated. The estimated disturbances are also given in Fig. 17. Specially, the fluctuations of the observed disturbances are caused by the varying of inductance and currents.

Figs. 18 and 19 show the current response comparison of the conventional and proposed DPCC schemes under flux ψ_f mismatch, respectively. Change progress of permanent flux is $\psi_f = 0.5\psi_{f0} \rightarrow \psi_{f0} \rightarrow 2\psi_{f0}$. Due to flux mismatch, the real q-axis current cannot track the reference q-axis current accurately, and the errors are obvious, as shown in Fig. 18. The current tracking error also increases with the speed. The flux mismatch mainly generates q-axis disturbance, too. As for

the proposed DPCC (Fig. 19), the disturbance caused by flux mismatch is observed by HSMO, and feedback to DPCC. Therefore, the steady-state current errors are eliminated. The estimated disturbances are also given in Fig. 19.

Figs. 20 and 21 show the current response comparison of the conventional and proposed DPCC under inductance L and flux ψ_f mismatch. Change progresses of inductance and flux are $L = 0.5L_0 \rightarrow L_0 \rightarrow 2L_0$ and $\psi_f = 0.5\psi_{f0} \rightarrow \psi_{f0} \rightarrow 2\psi_{f0}$. In this condition, the real d- and q-axis current cannot track the reference values accurately. Even worse, the dynamic performance of conventional DPCC is deteriorated significantly. As for the proposed DPCC (Fig. 21), the disturbances caused by inductance and flux mismatches are estimated by HSMO, and

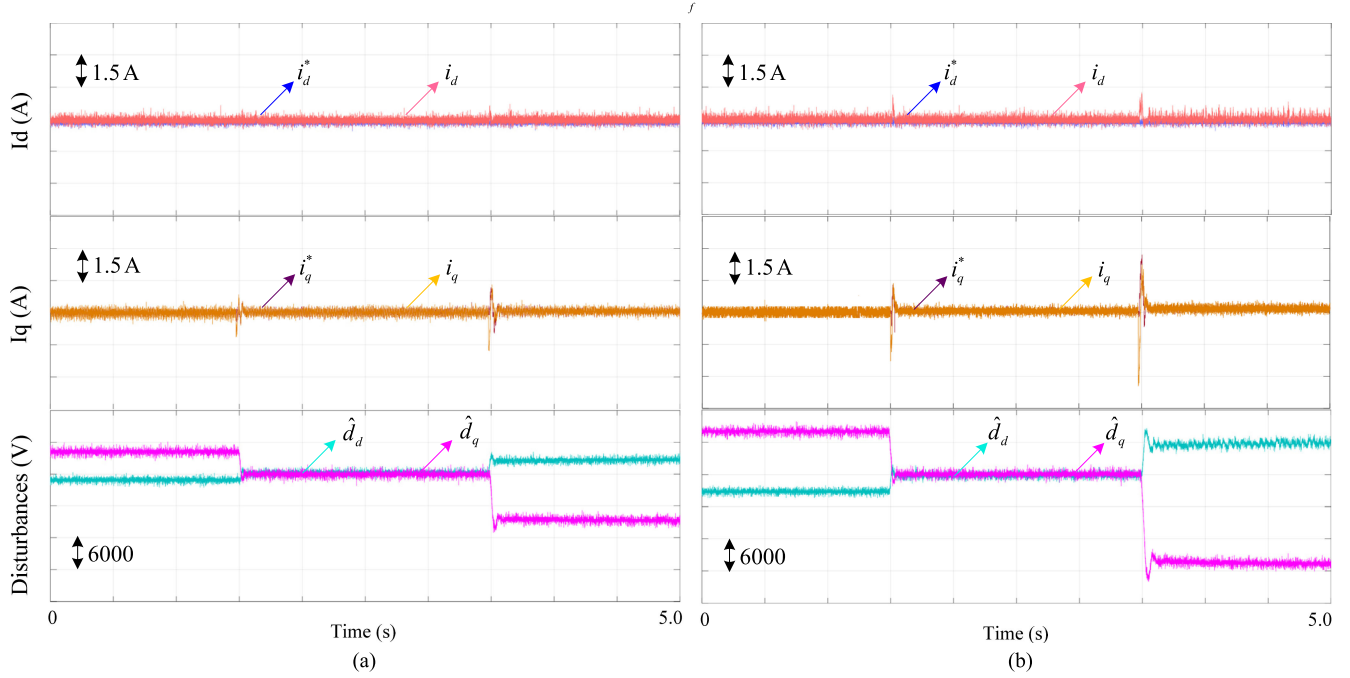


Fig. 21. Currents responses of the proposed DPCC under inductance L and flux ψ_f mismatch. (a) 500 rpm 10 Nm. (b) 1000 rpm 10 Nm.

feedbacked to DPCC. Therefore, the steady-state current error is eliminated. Meanwhile, the parameter robustness is improved. The estimated disturbances are given in Fig. 21.

VI. CONCLUSION

In this paper, one universal PMSM model includes the parameters variation and external disturbances is derived. And the SMC and DPCC are implemented in the speed and current loops of PMSM control scheme, respectively. Then, a unified high-order sliding mode observer is applied for the estimations of disturbances and uncertainties in speed, d - and q -axis current loops. The estimated disturbances are feedbacked to the proposed SMC and DPCC. Therefore, the proposed control strategy can achieve high-performance with acute variations of load and parameters. The effectiveness of the proposed control algorithm is verified by experimental results.

APPENDIX

A. PROOF OF THEOREM 2.1

Ignoring B and others, combine (5) and (6), it is given as

$$d\omega_e/dt = \dot{\omega}_e^* + c \cdot e_\omega + \int [\varepsilon \text{sgn}(s) + k \cdot s] + d_\omega(t) \quad (27)$$

Then, it can be written as

$$\dot{\omega}_e = \dot{\omega}_e^* + (c + k) \cdot e_\omega + kc \int e_\omega dt + \int \varepsilon \text{sgn}(s) dt + d_\omega(t) \quad (28)$$

By the modulation of sliding mode motion, the system can reach the stable state gradually, and the speed tracking error can converge to zero. (28) is modified as

$$\varepsilon \text{sgn}(s) = \dot{d}_\omega(t) \quad (29)$$

Therefore, ε is proportional to the derivative of $d_\omega(t)$.

B. PROOF OF THEOREM 4.1

Ignoring the disturbance $d_\omega(t)$, and take Laplace transportation of (28), it obtains

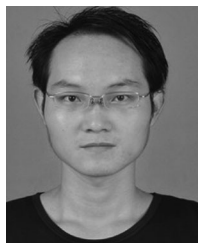
$$s \cdot \omega_e = s \cdot \omega_e^* + (c + k) \cdot e_\omega + kc \cdot e_\omega / s + \varepsilon \cdot |e_\omega| / s \cdot e_\omega \quad (30)$$

It is obvious that the proof is done. Meanwhile, $\varepsilon \cdot |e_\omega| / s \cdot e_\omega$ stands for the invariance of SMC.

REFERENCES

- [1] J. Zhang, H. Yao, and G. Rizzoni, "Fault diagnosis for electric drive systems of electrified vehicles based on structural analysis," *IEEE Trans. Veh. Technol.*, vol. 66, no. 2, pp. 1027–1039, Feb. 2017.
- [2] J. Druant, F. D. Belie, and P. Sergeant, "Field-oriented control for an induction-machine-based electrical variable transmission," *IEEE Trans. Veh. Technol.*, vol. 65, no. 6, pp. 4230–4240, Jun. 2016.
- [3] Y. Lin, K. Hu, and T. Yeh, "An electric-vehicle IPMSM drive with interleaved front-end DC/DC converter," *IEEE Trans. Veh. Technol.*, vol. 65, no. 6, pp. 4493–4504, Jun. 2016.
- [4] Y. Kung and M. Tsai, "FPGA-based speed control IC for PMSM drive with adaptive fuzzy control," *IEEE Trans. Power Electron.*, vol. 22, no. 6, pp. 2476–2486, Nov. 2007.
- [5] S. Kim, J. Lee, and K. Lee, "Offset-free robust adaptive back-stepping speed control for uncertain permanent magnet synchronous motor," *IEEE Trans. Power Electron.*, vol. 31, no. 10, pp. 7065–7076, Oct. 2016.
- [6] H. Liu and S. Li, "Speed control for PMSM servo system using predictive functional control and extended state observer," *IEEE Trans. Ind. Electron.*, vol. 59, no. 2, pp. 1171–1183, Jul. 2012.
- [7] Y. Jiang, W. Xu, and C. Mu, "Robust sliding mode speed control with adaptive torque observer for high performance PMSM," in *Proc. Int. Conf. Veh. Power Propulsion Conf.*, Oct. 2016, pp. 1–6.
- [8] Y. Feng, X. Yu, and F. Han, "High-order terminal sliding-mode observer for parameter estimation of a permanent-magnet synchronous motor," *IEEE Trans. Ind. Electron.*, vol. 60, no. 10, pp. 4272–4280, May 2013.

- [9] C. Mu, W. Xu, and C. Sun, "On switching manifold design for terminal sliding mode control," *J. Franklin Inst.*, vol. 353, no. 7, pp. 1553–1572, Feb. 2016.
- [10] Y. Zhang and H. Yang, "Two-vector-based model predictive torque control without weighting factors for induction motor drives," *IEEE Trans. Power Electron.*, vol. 31, no. 2, pp. 1381–1390, Sep. 2016.
- [11] B. Wang, X. Chen, and Y. Yu, "Robust predictive current control with online disturbance estimation for induction machine drives," *IEEE Trans. Power Electron.*, vol. 32, no. 6, pp. 4663–4674, Jun. 2017.
- [12] M. Yang, X. Lang, and J. Long, "A flux immunity robust predictive current control with incremental model and extended state observer for PMSM drive," *IEEE Trans. Power Electron.*, vol. 32, no. 12, pp. 9267–9279, Jan. 2017.
- [13] X. Zhang, B. Hou, and Y. Mei, "Deadbeat predictive current control of permanent-magnet synchronous motors with stator current and disturbance observer," *IEEE Trans. Power Electron.*, vol. 32, no. 5, pp. 3818–3834, May 2017.
- [14] J. Hu and Z. Zhu, "Improved voltage-vector sequences on dead-beat predictive direct power control of reversible three-phase grid-connected voltage-source converters," *IEEE Trans. Power Electron.*, vol. 28, no. 1, pp. 254–267, Jan. 2013.
- [15] J. Yang, W. Chen, and S. Li, "Disturbance/uncertainty estimation and attenuation techniques in PMSM drives—A survey," *IEEE Trans. Ind. Electron.*, vol. 64, no. 4, pp. 3273–3285, Apr. 2016.
- [16] A. Rabiei, T. Thiringer and M. Alatalo, "Improved maximum-torque-per-ampere algorithm accounting for core saturation, cross-coupling effect, and temperature for a PMSM intended for vehicular applications," *IEEE Trans. Transport. Electric.*, vol. 2, no. 2, pp. 150–159, Jun. 2016.
- [17] V. Ruuskanen, J. Nerg, and J. Pyrhönen, "Drive cycle analysis of a permanent-magnet traction motor based on magnetostatic finite-element analysis," *IEEE Trans. Veh. Technol.*, vol. 64, no. 3, pp. 1249–1254, Mar. 2015.
- [18] T. Li, X. Zou, and S. Feng, "SRF-PLL based sensor-less control strategy using improved dead-beat controller for direct-driven permanent magnet synchronous generator (PMSG)," in *Proc. Int. IEEE Appl. Power Electron. Conf. Expo.*, Mar. 2013, pp. 2984–2989.
- [19] T. Türker, U. Buyukkeles, and A. F. Bakan, "A robust predictive current controller for PMSM drives," *IEEE Trans. Ind. Electron.*, vol. 63, no. 6, pp. 3906–3914, Jan. 2016.
- [20] L. Niu, M. Yang, and D. Xu, "Predictive current control for permanent magnet synchronous motor based on deadbeat control," in *Proc. Int. IEEE Conf. Ind. Electron. Appl.*, Jul. 2012, pp. 46–51.
- [21] M. A. Haider, S. Saleh, R. Shao, and L. Chang, "Robust current controller for grid-connected voltage source inverter," in *Proc. Int. IEEE Int. Symp. Power Electron. Distrib. Gener. Syst.*, Apr. 2017, pp. 1–7.
- [22] W. Xu, Y. Jiang, and C. Mu, "Novel composite sliding mode control for PMSM drive system based on disturbance observer," *IEEE Trans. Appl. Supercond.*, vol. 26, no. 7, pp. 1–6, Oct. 2016.



Yajie Jiang received the B.S. degree from the School of Electrical Engineering, Zhengzhou University, Zhengzhou, China, in 2015. He is currently working toward the M.S. degree in the School of Electrical and Electronic Engineering, Huazhong University of Science and Technology, Wuhan, China.

His research interests include sliding mode control, permanent magnet synchronous machine control, disturbance observation technology, and advanced current control.



Wei Xu (M'09–SM'13) received the B.E. and M.E. degrees from Tianjin University, Tianjin, China, in 2002 and 2005, respectively, and the Ph.D. degree from the Chinese Academy of Sciences, Beijing, China, in 2008, all in electrical engineering. From 2008 to 2012, he held several academic positions with Australian and Japanese universities and companies. Since 2013, he has been a Full Professor with the State Key Laboratory of Advanced Electromagnetic Engineering and Technology, School of Electrical and Electronic Engineering, Huazhong University of Science and Technology, Wuhan, China. His research interests mainly include the electromagnetic design and control algorithms of linear/rotary machines, including induction, permanent magnet, switched reluctance, and other emerging novel structure machines.



Chaoxu Mu (M'15) received the Ph.D. degree in control science and engineering from Southeast University, Nanjing, China, in 2012. She was a Visiting Ph.D. Student with the Royal Melbourne Institute of Technology University, Melbourne, VIC, Australia, from October 2010 to November 2011. She was a Postdoctoral Fellow with the Department of Electrical, Computer and Biomedical Engineering, University of Rhode Island, Kingston, RI, USA, from December 2014 to August 2016. She is currently an Associate Professor in the School of Electrical and Information Engineering, Tianjin University, Tianjin, China. Her current research interests include nonlinear system control and optimization, and adaptive and learning systems.



Yi Liu (M'14) was born in Wuhan, China, in 1982. He received the B.S. and M.S. degrees in automation and control engineering from the Wuhan University of Science and Technology, Wuhan, China, in 2004 and 2007, respectively; and the Ph.D. degree in mechatronic engineering from the Huazhong University of Science and Technology, Wuhan, China, in 2016. From 2007 to 2011, he was a Lecturer at the Wuhan University of Science and Technology. From March 2016 to June 2016, he was a Senior R & D Engineer at the Fourth Academy of China Aerospace Science and Industry Group, Wuhan, China. In July 2016, he became a Postdoctoral Research Fellow in the School of Electrical and Electronic Engineering, Huazhong University of Science and Technology, Wuhan, China. His current research interests include ac electrical machine control and inverter systems.